Magnetic and related properties of the $CePd_{1-x}Rh_xAl$ system

A. Ślebarski, W. Głogowski, and J. Goraus
Institute of Physics, University of Silesia, 40-007 Katowice, Poland

D. Kaczorowski
Institute for Low Temperature and Structure Research, Polish Academy of Sciences, 50-950 Wrocław, Poland

(Received 15 October 2007; revised manuscript received 5 March 2008; published 28 March 2008)

In view of the contrasting behavior of the ternary compounds CePdAl and CeRhAl, the solid solutions $CePd_{1-x}Rh_xAl$ have been investigated in order to determine the dependence of their electronic structure properties on the number of conduction electrons. Magnetic susceptibility, electrical resistivity, and heat capacity studies revealed an evolution from an antiferromagnetic state at $x=0$ through short-range ordering for $0<x\leq 0.9$ to another antiferromagnetic state for $x>0.9$. Simultaneously, a crossover was found from the behavior characteristic for a Kondo lattice, seen for $x<0.6$, to a state in which the Kondo effect is nearly quenched (for larger x). The observed changes in the electronic structure across the $CePd_{1-x}Rh_xAl$ system have been corroborated by the results of x-ray photoemission spectroscopy.

DOI: 10.1103/PhysRevB.77.125135 PACS number(s): 71.27.+a, 75.40.Cx, 71.28.+d

I. INTRODUCTION

Ce-based Kondo-lattice intermetallics exhibit a variety of unusual ground states, including complex magnetic structures, heavy fermion (HF) states (both normal and superconducting), and paramagnetic insulating Kondo lattices. The reason for such a diversity of physical phenomena is a delicate interplay between two competing mechanisms: the local on-site Kondo effect and the long-range Ruderman-Kittel-Kasuya-Yoshida (RKKY) interaction. The result of this competition was first discussed by Doniach on the basis of the Kondo-lattice model Hamiltonian.[1] The simple phase diagram presents the magnetic ordering temperature T_{RKKY} vs $J_{fc}N(\epsilon_F)$ and displays a quantum critical point (QCP) at a critical value of $J_{fc}N(\epsilon_F)$, where $J_{fc}\sim V$ represents the strength of the exchange interaction between f and conduction electrons, $N(\epsilon_F)$ is the density of states (DOS) at the Fermi level, and V is the on-site hybridization energy among f and conduction electrons. The diagram, however, does not explain the character of the low-temperature magnetic ground state, because of its simplicity. In the Kondo-lattice limit, the stability of different ground states is strongly dependent on the on-site hybridization strength V, the bare f-level position in the conduction band, E_f, the number of electrons per atom, n_e, and the magnitude of the on-site Coulomb interaction U within the shell. Doradziński and Spałek[2] (DS) discussed the magnetic phases in the periodic Anderson model and constructed the magnetic phase diagram on the V-n_e plane. This diagram has been shown to give a good qualitative account of experimental results on the series of Ce ternary intermetallics.[3] For an even number of electrons per atom ($n_e=2$), it predicts paramagnetic Kondo insulator state with large hybridization V of bare f- and conduction-electron states, as is the case of CeRhSb and CeNiSn. In turn, CeRhAl lies on the V-n_e diagram on the line which separates antiferromagnetic and ferromagnetic metallic phases. The competition between these two different magnetic states can lead to the non-Fermi-liquid (NFL) behavior, recently observed indeed in CeRhAl.[4]

In the series of ternary intermetallic compounds, CeRhSb or CeNiSn, CePdAl, and CeRhAl, the number of valence electrons per formula unit is 18, 17, and 16, respectively. A paramagnetic Kondo insulator discussed within the periodic Anderson model provides an insulating state for a **k**-independent hybridization and for an even number of strongly correlated electrons per unit cell.[2] Additionally, the numerical calculations show that the Kondo gap depends strongly on the magnitude of hybridization between Ce $4f$ and the transition metal d states,[5] since the Ce $4f$ and Sn or Sb $5p$ mixing is small. In the case of the momentum-dependent hybridization V_k, the gap may vanish at either some points or along the lines where $V_k=0$, providing thus a semimetallic ground state of the system. In this series, CeRhAl is expected to be an insulator; this is, however, not the case.[6] Actually, the compound has a nonzero value of the DOS at the Fermi level[4] and is located on the V-n_e plane far from the paramagnetic Kondo insulator phase.[3] In turn, CePdAl is an antiferromagnetically ordered ($T_N=2.7$ K) HF compound,[7–9] which exhibits coexistence of 2/3 magnetically ordered Ce^{3+} moments with 1/3 frustrated disordered moments.[10] It was also shown[11,12] that CePdAl is very near to the crossover from the magnetic to the nonmagnetic regime.

In view of the diverse behavior of CePdAl with respect to that of CeRhAl, it is of interest to examine the solid solution between these two compounds, to see the effect of a decreasing number of valence band states (conduction states, if one treats the d electrons as almost localized) on the ground state properties. The aim of the present work was to investigate the magnetic and related properties of the $CePd_{1-x}Rh_xAl$ series by means of ac and dc magnetic susceptibility, heat capacity, and electrical resistivity measurements. Moreover, the electronic structure of these alloys was studied by x-ray photoemission spectroscopy (XPS) and the obtained valence band spectra were compared with the results of *ab initio* band structure calculations. The hybridization energy between the Ce $4f$ shell and the conduction band states, and the occupation number of the f shell, n_f, were estimated based on the Gunnarsson-Schönhammer theoretical model.[13] The experimental and calculated results are discussed here in terms of formation at low temperatures of a spin-glass state.

TABLE I. $CePd_{1-x}Rh_xAl$: structural properties, hybridization energy Δ obtained from the Ce $3d$ XPS spectra, $V=\{\Delta/[\pi N(\epsilon_F)]\}^{1/2}$, and the Sommerfeld coefficient γ obtained experimentally.

x	Symmetry	a, b, c (Å)			Δ (meV)	V (meV)	γ (mJ/mol K^2)
0	$P\bar{6}2m$	7.218,		4.229	210	150	70
0.2	*Pnma*	7.209,	4.281,	16.192	180		80
0.4	*Pnma*	7.195,	4.277,	16.133	200	120	60
0.5	*Pnma*	7.182,	4.268,	16.097	50	60	
0.6	*Pnma*	7.168,	4.253,	16.046	190		74
0.8	*Pnma*	7.124,	4.235,	15.965	180		96
0.9	*Pnma*	7.118,	4.232,	15.963	150		
0.95	*Pnma*	7.105,	4.220,	15.941	160		
1	*Pnma*	7.102,	4.213,	15.939	70	70	92

II. EXPERIMENTAL DETAILS

Polycrystalline samples of $CePd_{1-x}Rh_xAl$ were prepared by arc melting the stoichiometric amounts of the elemental constituents (Ce 99.99, Pd 99.99, Rh 99.95, and Al 99.999 at. %) on a water-cooled copper hearth in high-purity Ar atmosphere gettered by a melting Al ingot. The samples were remelted several times to promote homogeneity and subsequently annealed at 800 °C for 3 weeks. X-ray diffraction measurements showed only single phases. The x-ray pattern of CePdAl was fully indexed within a hexagonal unit cell of the ZrNiAl type (space group $P\bar{6}2m$), in agreement with the literature data.[7] All the other $CePd_{1-x}Rh_xAl$ samples with $0.2 \leq x \leq 1$ were found to crystallize with orthorhombic unit cells of the $Pd_2(MnPd)Ge_2$ type (space group *Pnma*). The lattice parameters were acquired from the diffraction patterns using the POWDER-CELL program[14] and they are listed in Table I.

The x-ray photoelectron spectroscopy spectra were obtained with monochromatized Al $K\alpha$ radiation using a PHI 5700 ESCA spectrometer. The samples were scraped with a diamond file under high vacuum immediately before taking a spectrum.

The ac magnetic susceptibility was measured in the 1.8–300 K temperature interval using a Lake-Shore susceptometer. The amplitude of the excitation field was 1 mT at a fixed frequency of 10 kHz. dc magnetic measurements were carried out in the temperature range from 1.8 to 300 K in applied magnetic fields up to 50 kOe employing a Quantum Design superconducting quantum interference device (SQUID) magnetometer. Electrical resistivity measurements were made in the range 2–300 K using a homemade setup and standard four-wire technique. The specific heat was measured by the adiabatic method between 2.7 and 70 K and in magnetic fields up to 70 kOe using a homemade calorimeter. Moreover, for selected samples the electrical resistivity and the specific heat were studied over the temperature interval 300 mK–10 K employing a Quantum Design physical properties measurement system (PPMS) platform equipped with a 90 kOe superconducting magnet.

The electronic structures of the compounds CePdAl and CeRhAl, as well as that of the mixed alloy $CePd_{0.5}Rh_{0.5}Al$, were studied by full potential linearized augmented plane wave (FPLAPW) methods.[15] The calculations were scalar relativistic and spin polarized. The general gradient approximation[16] (GGA96) was applied to account for the inhomogeneities of electronic charge density. Muffin-tin spheres with radii of 2.50, 2.50, 2.50, and 2.28 a.u. were assumed for Ce, Pd, Rh, and Al atoms, respectively. All the electronic structure calculations were performed using the experimental lattice parameters. Obviously, such an oversimplified treatment cannot properly account for the ground state properties of the $CePd_{1-x}Rh_xAl$ alloys, and hence the results of the numerical calculations are not meaningful in this respect. However, they can be used to calculate the theoretical valence band spectra, because these concern the Pd and Rh d-electron states, which decide the energy position and the overall shape of the main feature in the XPS response (see below). For this purpose the densities of states were convoluted by the Lorentzians with a full width at half maximum (FWHM) of 0.4 eV to account for the instrumental resolution and thermal broadening. The partial l-resolved densities of states were multiplied by the corresponding cross sections[17] and by the Fermi-Dirac function for 300 K.

III. RESULTS AND DISCUSSION

A. Magnetic, electrical transport, and thermal properties

Figure 1 displays the temperature dependencies of the ac magnetic susceptibility χ_{ac} of the series $CePd_{1-x}Rh_xAl$. The susceptibility of CePdAl exhibits a clear maximum at $T_N = 2.7$ K, similar to that observed previously by others,[7–9] which suggests an antiferromagnetic ordering below T_N. The recent studies showed, however, that this anomaly may alternatively manifest a spin-glass freezing that arises due to structural disorder in a Kagomé-like lattice.[18] Apparently such an anomaly is absent above 1.8 K for the samples with $0.2 \leq x < 0.95$. The observed suppression of the susceptibility maximum is similar to that recently reported for the $CePd_{1-x}Ni_xAl$ system for which the critical concentration of Ni was ~10%. Interestingly, the $\chi_{ac}(T)$ curves measured for $0.4 \leq x \leq 0.9$ show at low temperatures a divergent behavior (see the insets to Fig. 1). The susceptibility of the sample

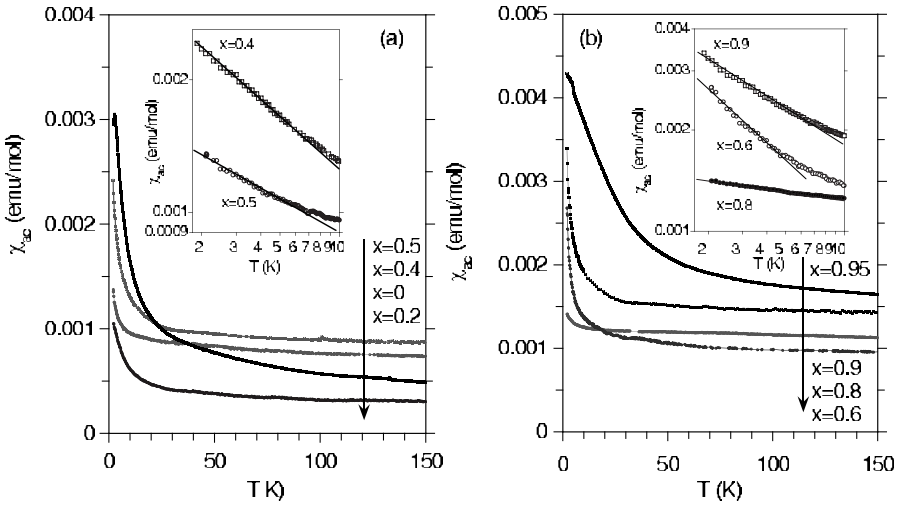

FIG. 1. ac magnetic susceptibility vs temperature for the series $CePd_{1-x}Rh_xAl$ with linear and logarithmic (the insets) temperature scales.

with 95% Rh shows a weak anomaly near 4.5 K which is very similar in character to that reported recently for pure CeRhAl.[4]

Shown in Fig. 2 are the temperature variations of the dc magnetic susceptibility χ and its inverse χ^{-1} measured for $CePd_{0.6}Rh_{0.4}Al$ and CeRhAl. The magnetic susceptibility data of $CePd_{0.6}Rh_{0.4}Al$ obey, in the entire temperature range studied, the modified Curie-Weiss law with an effective magnetic moment of $2.1\mu_B$, paramagnetic Curie temperature $\theta=-6$ K, and temperature-independent term $\chi_0=2.2\times10^{-3}$ emu/mol. Above 200 K the $\chi^{-1}(T)$ curve shows a straight-line behavior with $\mu_{\text{eff}}=2.60\mu_B$, i.e., close to the free ion value for Ce^{3+} $(2.54\mu_B)$, and θ being as large as -114 K (note the dashed line in Fig. 2). The field variation of the magnetization M taken at 1.8 K, presented in the inset to Fig. 2, is linear in fields $\mu_0H<3$ T, and only slightly deviates from linearity in higher fields. This behavior is distinctly

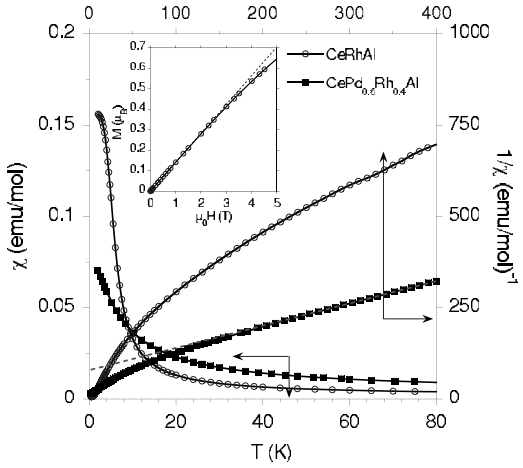

FIG. 2. dc magnetic susceptibility and its inverse vs temperature (note different scales) for $CePd_{0.6}Rh_{0.4}Al$ and CeRhAl. The dashed and solid lines through the $\chi^{-1}(T)$ data are the Curie-Weiss and the modified Curie-Weiss fits, respectively. The inset shows the magnetization M versus magnetic field measured for $CePd_{0.6}Rh_{0.4}Al$ at $T=1.8$ K. The dashed line emphasizes the straight-line behavior below 3 T.

different from that observed for the $CePd_{1-x}Rh_x$ alloys with $x<0.8$, which exhibit ferromagnetic ordering at low temperatures.[19,20]

The temperature dependence of χ^{-1} of CeRhAl shows a pronounced curvature up to 400 K and can be described by the modified Curie-Weiss formula with the fitting parameters $\mu_{\text{eff}}=1.57\mu_B$, $\theta=-11.3$ K, and $\chi_0=7\times10^{-4}$ emu/mol. The effective magnetic moment thus calculated is considerably smaller than the Ce^{3+} free ion value. The magnetic bulk data are thus in line with the scenario of a mixed valence state of Ce atoms in this compound, which is discussed below.

Figure 3 displays the temperature dependencies of the electrical resistivity of the $CePd_{1-x}Rh_xAl$ samples with $x\leq0.6$, Fig. 3(a), and $x\geq0.8$, Fig. 3(b). These data exhibit two qualitatively different temperature variations characteristic for the samples displayed in Figs. 3(a) and 3(b), respectively. The samples with $x\leq0.6$ show a Kondo-like behavior with a characteristic minimum in $\rho(T)$ occurring at $T_{\text{min}}\approx30$ K, which somewhat depends on the concentration x, and a logarithmic increase of the resistivity for $T\rightarrow T_{\text{max}}$. For CePdAl the $\rho(T)$ curve shows a Kondo-type maximum at a temperature $T_{\text{max}}=6$ K, which is much higher than T_N. On the other hand, if the maximum seen in $\chi_{\text{ac}}(T)$ at 2.7 K arises due to spin-glass freezing,[18] then the value of $T_{\text{max}}\approx2T_N$ could be explained by an interplay of spin-glass properties and the Kondo effect.[21,22] Actually, the resistivity of $CePd_{0.5}Rh_{0.5}Al$ varies proportionally to $T^{3/2}$ in the temperature range 300 mK–1 K, and it decreases linearly with T in the range $3.5<T<12$ K. Such behavior is typical for spin glasses below and above the resistivity maximum, respectively, that is related to the spin freezing temperature T_f. The $T^{3/2}$ power law qualitatively corresponds to the effects of frozen-in disorder, as observed, for example, in amorphous metals and polycrystalline spin glasses,[23] which is expected to lead to a diffusive motion of charge carriers on length scales substantially larger than the mean free path.[24,25] Alternatively, the $\rho\sim T^{3/2}$ variations can be interpreted in the framework of nearly ferromagnetic Fermi-liquid models,[26] as recently discussed for the itinerant-electron ferromagnets $ZrZn_2$ (Ref. 27) and Ni_3Al.[28] In the case of CeRhAl, however, the latter scenario should be ruled out, because of the absence of any hints at ferromagnetism coming from the bulk magnetization data (see Fig. 2).

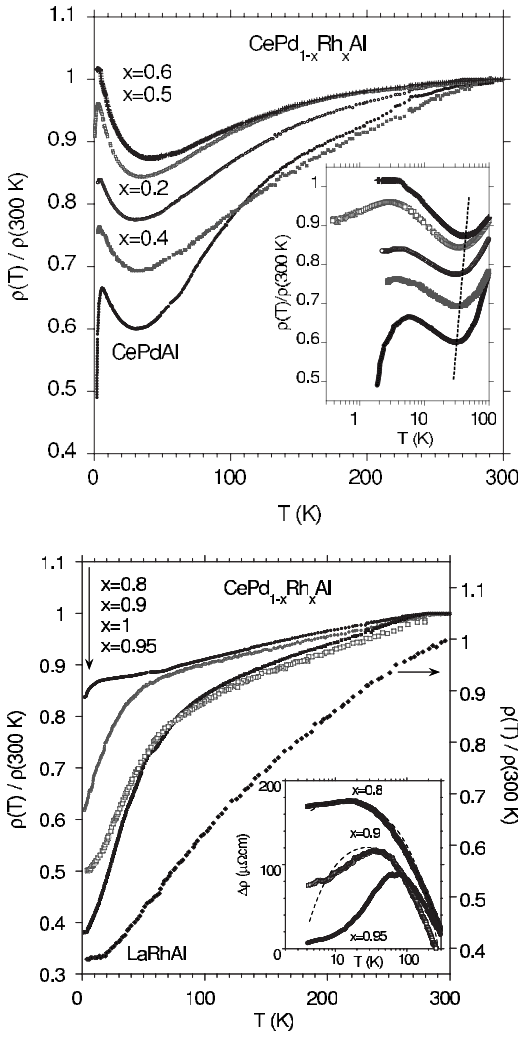

FIG. 3. Temperature dependencies of the resistivity of the $CePd_{1-x}Rh_xAl$ alloys, normalized to the room temperature values. The inset in (a) shows the resistivity on a logarithmic scale. The inset in (b) displays $\Delta\rho=\rho(CePd_{1-x}Rh_xAl)-\rho(LaRhAl)$ on a semilogarithmic scale. The $\Delta\rho$ data for the samples with $x=0.8$ and 0.9 are fitted by the formula $\Delta\rho=a-bT-c/T$ with the residual resistivity $a=190$ and 160 $\mu\Omega$ cm for the former and the latter alloy, respectively, the modified phonon term $b=0.6$ $\mu\Omega$ cm/K for both samples, and the coefficient $c=117$ and 535 $\mu\Omega$ cm K, for the samples with $x=0.8$ and 0.9, respectively.

It should be noted that the upturns in $\rho(T)$ found for the $CePd_{1-x}Rh_xAl$ samples with $x\leq 0.6$ cannot be interpreted in terms of a simple activated behavior. Consistent with this finding are the results of band structure calculations, which did not reveal the presence of any energy gap for these phases (see below). Instead, the resistivity in the temperature range $7<T<27$ K can be well described by a two-channel conduction model, in which one considers a temperature-independent term that accounts for the occurrence of a pseudogap in the density of states near the Fermi level and a Mott term $\rho\sim\exp(T_0/T)^{1/4}$ that describes variable-range hopping (VRH) of carriers between localized states.[29] The $\ln\rho$ versus $T^{-1/4}$ plots of the experimental data of the alloys with $x\leq 0.6$ display a linear behavior between ~7 and ~27 K (not shown). The VRH mechanism was found to dominate the electronic transport in the Pauli paramagnets ZrNiSn and TiNiSn (Ref. 30) as well as ThPtSn,[31] and the two-channel model was successfully applied to the case of the resistivity behavior of PuTe measured under high pressure.[32]

The $\rho(T)$ curves displayed in Fig. 3(b) are qualitatively different in comparison to those measured for the alloys with $x\leq 0.6$. The resistivity of the samples with $x\geq 0.8$ varies proportionally to $T^{3/2}$ at low temperatures, as usually observed for $T<T_f$ in diluted metallic spin glasses.[23] The temperature interval in which the $\rho(T)\sim T^{3/2}$ behavior was found is $4.3<T<29$ K, $T<10$ K, and $T<3.5$ K for the sample with 95%, 90%, and 80% of Rh atoms, respectively. The inset in Fig. 3(b) displays the resistivity of these alloys upon subtracting the resistivity of the compound LaRhAl with no f electrons. The apparent maxima in $\Delta\rho(T)$ can be explained in two ways: (i) it can result from an interplay of the spin-glass behavior and the Kondo effect,[21,22] or (ii) the Kondo effect is negligible[33] and the maximum arises due to the combined effect of a modified-phonon contribution $\Delta\rho_{ph}\sim -bT$ as the impurity atoms differ in valence (charge density) and size from the host, and the RKKY spin-flip scattering contribution $\Delta\rho_{RKKY}\equiv -c/T=m^\star/(ne^2\tau_{RKKY})$.[34] In the second scenario the impurity resistivity is related to the scattering time τ_{RKKY}, where $m^\star$ is the effective electron mass, e is the electron charge, and n denotes the electron density. As shown in the inset to Fig. 3(b), the formula $\Delta\rho=a-bT-c/T$ describes well the maximum in $\Delta\rho$ observed for the samples with $x=0.8$ and 0.9. However, the resistivity of the alloy with 95% Rh and that of pure CeRhAl cannot be interpreted within this expression. The $\Delta\rho$ curves of both samples exhibit a maximum at $T_m\approx 80$ K that probably manifests the coherence effect, and a clear logarithmic decrease for $T>100$ K, both features being expected for Kondo lattices. Alternatively, the maximum in $\Delta\rho$ can be attributed to an interplay of the crystal-electric field (CEF) effect and the Kondo effect,[35,36] as suggested recently for CeRhAl (for details see Ref. 4).

The results of specific heat measurements performed on two characteristic samples from the $CePd_{1-x}Rh_xAl$ series, namely, for $CePd_{0.2}Rh_{0.8}Al$ and $CePd_{0.8}Rh_{0.2}Al$, are shown in Fig. 4. For both alloys, the ratio C/T follows at low temperatures (below about 8 K) a power-law behavior $C/T\sim T^{-n}$ with the exponent $n=0.25$ for the former composition and $n=1.2$ for the latter. The exponent $n\approx 1$ was found also for other samples with $x=0.4$ and 0.6. In contrast, for pure CePdAl the specific heat data[8,37] display an onset of magnetic fluctuations expected in the magnetic chain for $T>T_N$ (see Ref. 38) with a T^{-2} dependence of $C_m(T)$. Similarly, for the other terminal compound, i.e., CeRhAl, a λ-type anomaly in $C(T)$ indicates the onset of antiferromagnetic ordering.[4] Clearly, the Rh concentration of ~80% seems to separate the spin-glass-like behavior for the Rh content $0.2\leq x<0.8$ and the antiferromagnetic ordering that occurs for $x>0.9$.

The C/T vs T^2 plot of the data measured for $CePd_{0.8}Rh_{0.2}Al$, shown in the inset to Fig. 4, yields for $T\rightarrow 0$ a rather large value for the linear specific heat coefficient, $\gamma=\gamma_{el}+\gamma_m=80$ mJ/(mole K^2), where γ_{el} denotes the electronic contribution and γ_m stands for the magnetic contribution. A similarly enhanced γ was found also for the

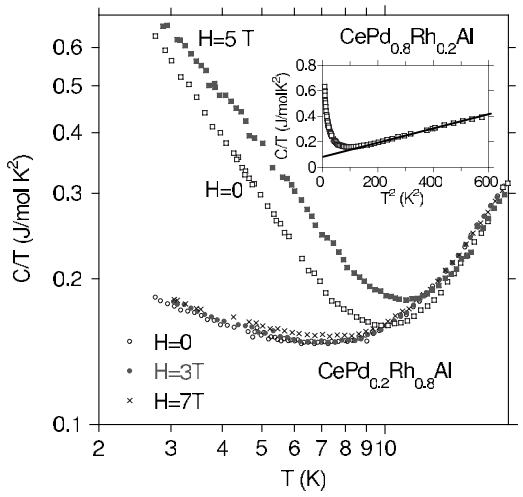

FIG. 4. Specific heat divided by temperature, C/T, versus temperature on a log-log scale taken at different magnetic fields for $CePd_{0.8}Rh_{0.2}Al$ and for $CePd_{0.2}Rh_{0.8}Al$. The inset shows C/T vs T^2 for $CePd_{0.8}Rh_{0.2}Al$ measured in zero field.

other alloys from this series (see Table I). Although coexistence of HF behavior and spin-glass freezing has been reported for several ternary intermetallics [e.g., URh_2Ge_2,[39] U_2PdSi_3,[40] CeAgAl (Ref. 41)], it is impossible to separate the two linear contributions to the specific heat data, and hence unambiguously draw conclusions about possible HF character in the materials studied.

The low-temperature specific heat of $CePd_{0.4}Rh_{0.6}Al$ measured in different applied magnetic fields is shown in Fig. 5(a) in the form of C versus T and in Fig. 5(b) as C/T versus T (the latter in a logarithmic scale). The $C(T)$ curve is dominated by a broad hump that is located at ~ 2.8 K in zero field and slightly shifts to higher temperatures with rising field strength up to $\mu_0 H = 6$ T. In stronger fields the change in $C(T)$ is more evident. At low temperatures the specific heat is roughly a linear function of T. Qualitatively the $C(T)$ data in Fig. 5 are reminiscent of spin-glass behavior,[42] as observed for several classical spin glasses, like, e.g., CuMn alloys.[43] It is worth noting that for $T < 2$ K the magnetic contribution to the specific heat ΔC cannot be described by the expression appropriate for an anisotropic magnetic system with a gap δ in the magnon dispersion: $\Delta C = AT^n e^{-\delta/T}$, where $n=3$ for antiferromagnetic or $n=3/2$ for ferromagnetic interactions. The overall behavior of the specific heat of $CePd_{0.4}Rh_{0.6}Al$ may also be discussed in the context of the Kondo effect.[44] Indeed, the C/T data shown in Fig. 5(b) are similar to those reported for various Kondo systems.[45,46] The maximum observed in zero field at 340 mK presumably manifests an onset of long-range magnetic order that replaces the spin-glass state present at higher temperatures.

Figure 6 shows the nonlattice contribution $\Delta C = C(CePd_{1-x}Rh_xAl) - C(LaRhAl)$ to the specific heat for a few compositions x, derived assuming that the phonon contribution C_{ph} to the specific heat of LaRhAl is a good approximation of C_{ph} in the Ce compounds.[48] The ΔC curve obtained for CeRhAl was deconvoluted for $T > T_N$ into three terms $\Delta C = C_{el} + C_K + C_{Sch}$. In this analysis the CEF doublet-

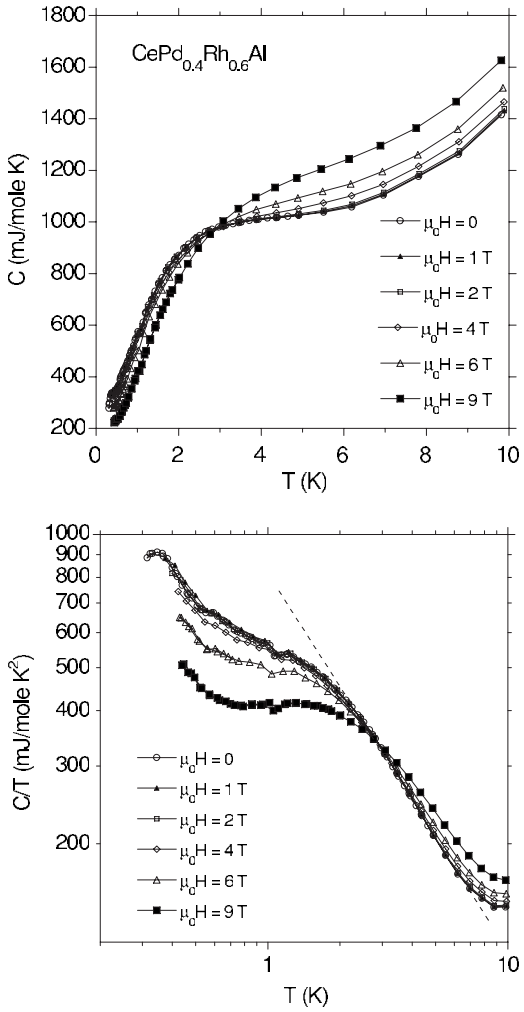

FIG. 5. Temperature dependence of the specific heat of $CePd_{0.4}Rh_{0.6}Al$ (a), and the ratio C/T vs T (b), measured at several different magnetic fields.

doublet scheme was accepted with the energy separations $\Delta_1 = 103$ K and $\Delta_2 = 140$ K, as derived in Ref. 4, and the Kondo contribution was calculated according to the theory by Desgranges and Schotte.[47] For the other alloys the maxima in the ΔC vs T dependence can be attributed to the CEF effect with a similar energy level scheme; however, the magnitude of the excess specific heat below ~ 10 K is much smaller than the calculated Kondo contribution C_K. This finding confirms the hypothesis formulated above on the basis of the resistivity results that the $CePd_{1-x}Rh_xAl$ alloys with $0.8 \leq x < 0.95$ exhibit rather weak Kondo screening effect.

In conclusion, the low-temperature experimental data for the $CePd_{1-x}Rh_xAl$ series reveal that long-range antiferromagnetic order develops in CePdAl and in the Rh rich samples with $x \geq 0.95$, whereas for the intermediate compositions short-range magnetic correlations are observed to prevail, which lead to inhomogeneous magnetic states. The specific heat coefficient γ is ~ 80 mJ/mol K^2 for all samples from the concentration range $0.2 \leq x < 0.8$, and the $C(T)$ and $\rho(T)$ variations exhibit features typical for spin-glass systems. The paramagnetic Curie temperature θ extrapolated from the tem-

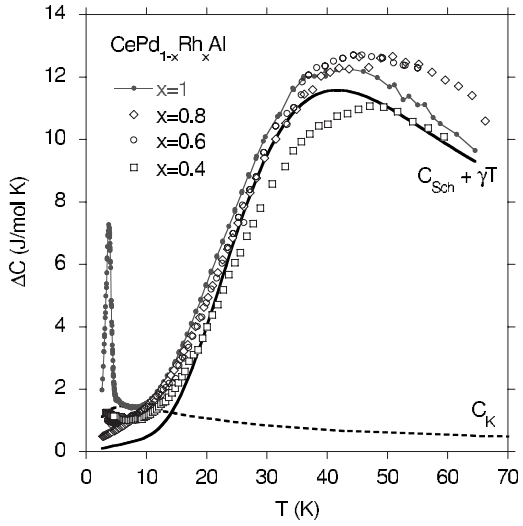

FIG. 6. Temperature dependence of the nonlattice contribution $\Delta C = C(\text{Ce sample}) - C(\text{LaRhAl})$ to the specific heat of $CePd_{1-x}Rh_xAl$. The solid line is a sum of the free electron (C_{el}) and Schottky (C_{Sch}) contributions and the dotted curve is the Kondo contribution (C_K) to the specific heat of CeRhAl.

perature region $T > 200$ K is negative and of the order of ~ -100 K (see an example in Fig. 2), which suggests an interplay of the magnetic interactions between the Ce moments and the Kondo effect. The standard single-impurity Kondo model predicts $T_K \approx |\theta|/4$,[49] which yields a reasonable estimate for the Kondo temperature $T_K \approx 20-25$ K. These values of T_K roughly correlate with the values of T_{min} at which the $\rho(T)$ curves show minima (see Fig. 3).

For the terminal compound CeRhAl and the alloy $CePd_{0.05}Rh_{0.95}Al$ one observes a resistivity maximum at $T_{max} \sim 80$ K and a $\rho \sim -\ln T$ dependence at higher temperatures [see the inset in Fig. 3(b)]. This behavior is characteristic of Kondo lattices with coherence effect below T_{max}. The standard expression for the virtual bound state width[50] predicts that $k_B T_{max} \sim \pi V^2 N(\epsilon_F)$, where V is the magnitude of intra-atomic hybridization of the f states with the conduction electrons and $N(\epsilon_F)$ is the density of states in the bare conduction band at the Fermi energy. Assuming typical values $N(\epsilon_F) \sim 1/3$ (eV atom)$^{-1}$ and $V \sim 0.07$ eV (see Table I), one obtains $T_{max} \sim 60$ K, which agrees reasonably well with the experimental findings. Competition between the Kondo effect and the spin-glass freezing at $x = 0.8$ seems to divide the entire $CePd_{1-x}Rh_xAl$ series into two composition ranges: one with dominant Kondo interactions (for larger x) and the other with predominance of spin-glass features (for smaller x). For the alloy $CePd_{0.2}Rh_{0.8}Al$ one observes $C/T \sim T^{-n}$, where n is only $\sim 1/5$ of that obtained for the samples with $0 < x < 0.8$, and the resistivity of this alloy follows the formula appropriate for spin glasses with weak Kondo interactions (see the discussion above).

B. Electronic structure

Ce core level photoemission is an appropriate method to get insight into the character of the Ce $4f$ states in Ce-based intermetallics owing to the strong Coulomb interaction between the photoemission core hole and the electrons located near the Fermi level. This coupling results in a complex structure of the Ce-core level XPS spectra.[13] Figure 7(a) shows the Ce $3d$ XPS spectra obtained for the series $CePd_{1-x}Rh_xAl$ (background, calculated using the Tougaard algorithm,[51] was subtracted from the experimental data). The separation of the overlapping peaks in the spectrum was done on the basis of the Doniach-Šunjić theory.[52] The spin-orbit (SO) interaction results in two sets of Ce $3d$ photoemission lines in the XPS spectrum, which are assigned to the $3d_{3/2}$ and $3d_{5/2}$ components of the final states. Each SO set of the Ce $3d$ XPS lines can consist of contributions marked as f^0, f^1, and f^2. The main peaks $3d^9f^1$ originate from Ce^{3+}. The $3d^9f^2$ final state components appear when the core hole becomes screened by an additional $4f$ electron due to the hybridization of the Ce $4f$ shell with the conduction band. Consequently, the contribution of the $3d^9f^2$ lines in the measured Ce $3d$ spectrum reflects the hybridization strength, Δ

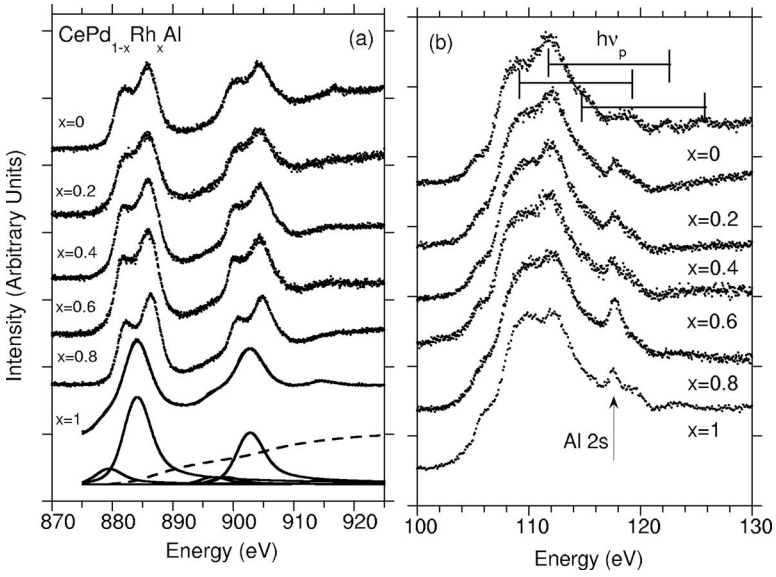

FIG. 7. Ce $3d$ XPS (a) and Ce $4d$ XPS (b) spectra obtained for $CePd_{1-x}Rh_xAl$. The f^0, f^1, and f^2 components in (a) are separated on the basis of the Doniach-Šunjić theory. As an example is shown the result of deconvolution of the Ce $3d$ XPS spectra of CeRhAl ($x=1$) with the spin-orbit splitting of 18.6 eV. The experimental data (points) are very well fitted (line) by the sum of the deconvoluted lines $3d_j^9f^2$, $3d_j^9f^1$, and $3d_j^9f^0$, where $j = 5/2, 3/2$, which are displayed in the bottom of (a). The satellite lines observed in the $3d$ XPS spectra of CePdAl are interpreted as plasmon losses with energy of $\hbar\omega_p \approx 11$ eV.

$=\pi V^2 N(\epsilon_F)$. The presence of the $3d^9f^0$ component clearly indicates an intermediate valence character of the Ce ions. The quantitative analysis was performed based on the Gunnarsson and Schönhammer (GS) theory.[13] The details of the method were described elsewhere.[53] It is worthwhile to stress that the measured Ce 3*d* XPS spectra represent the total signal from all of the Ce atoms. In the samples $CePd_{1-x}Rh_xAl$ with $x \geq 0.2$ there are two crystallographic positions occupied by Ce atoms. The Ce atoms in nonequivalent positions have different local environments, which can lead to different chemical shifts of the respective photoemission lines. Recently, we have shown that these shifts are of the order of 0.1 eV, and they are much smaller than the intervals between the f^1 and f^2 final state contributions in the Ce 3*d* XPS spectrum.[54] We therefore interpret the estimated Δ value as the average hybridization energy for the two Ce atoms. The Δ value is ~200 meV for CePdAl, and ~190 meV for $CePd_{1-x}Rh_xAl$ samples with $1 > x \geq 0.2$, whereas for CeRhAl the hybridization energy drastically decreases and is about 70 meV.[55]

The 4*f* occupation number in CeRhAl is $n_f = 0.9$, whereas for the other $CePd_{1-x}Rh_xAl$ alloys $n_f \rightarrow 1$. The peak located at ~917 eV at the high-energy side of the f^1 component [see Fig. 7(a)] in the 3*d* XPS spectra of CePdAl should be attributed to plasmon losses arising from group oscillations of the conduction electrons ($\hbar\omega_p \cong 11$ eV). The same energy plasmons are visible in the Ce 4*d* XPS spectrum of CePdAl [see Fig. 7(b)]. There is other evidence for fluctuating valence of Ce in CeRhAl, as shown in Fig. 7(b). The Ce 4*d* XPS spectra of CeRhAl exhibit two peaks at ~119 and 123 eV which can be assigned to the f^0 final state.[56] The indicated splitting 3.1 eV has almost the same magnitude as the spin-orbit splitting of the La 4*d* states.

Figure 8 shows the XPS valence band (VB) spectra for the series of $CePd_{1-x}Rh_xAl$ alloys. Each spectrum exhibits a maximum that originates mainly from the Pd *d* states. A band located in the binding energy range of ~5–7 eV originates from the *s* states of Al.The VB XPS intensities distributed near the Fermi level result from the occupied Ce 4*f* states, but there is some contribution of the Pd *d* states and the Al *p* states. For CePdAl the hybridization energy $V = \{\Delta/[\pi N(\epsilon_F)]\}^{1/2}$ is about 150 meV. According to the Anderson model, $J_{fc} \sim -|V|^2/E_{4f} \approx 0.1$ eV, if the 4*f* states are located near ϵ_F in the band. From this value one obtains $|N(\epsilon_F)J_{fc}| > 0.3$, which locates CePdAl on the left side of the Doniach phase diagram, near the maximum in the T_N vs $|N(\epsilon_F)J_{fc}|$ function, in agreement with Ref. 37. The strength of the *f*-*c* exchange interaction can, however, be tuned by changes in composition or external pressure, and by these means influence the competition between the intrasite Kondo and intersite Ruderman-Kittel-Kasuya-Yoshida interactions. The investigations of the resistivity of CePdAl under external pressure confirmed that this compound is very near to the crossover from the magnetic to the nonmagnetic regime.[11,12]

In the Doradziński-Spałek model the stability of the paramagnetic vs the magnetic ground state in the Kondo-lattice limit is strongly dependent on the on-site hybridization magnitude *V*, the bare *f*-level position, and the number of conduction electrons n_e. Based on our XPS data, the DS phase diagram on the V-n_e plane ($n_e = n_f + n_c \rightarrow 2$ is the total number of electrons per site) describes CePdAl as an antiferromagnetic Kondo-lattice compound.

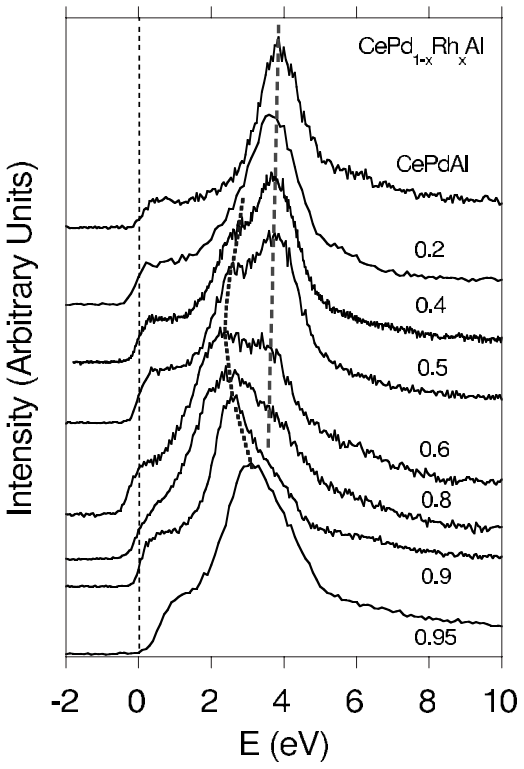

FIG. 8. Valence XPS bands for $CePd_{1-x}Rh_xAl$. The dotted lines show the maxima of the *d* VB XPS spectra of Pd and Rh, respectively.

As is apparent from Fig. 8, the maximum observed in the XPS VB spectrum of CePdAl slightly shifts to lower binding energies when Pd is substituted by Rh. With increasing Rh content, the second maximum appears at ~2.5 eV, and its location in the conduction band of the series $CePd_{1-x}Rh_xAl$ is dependent on *x*. Figure 9 compares the calculated LAPW XPS bands and the experimental XPS VB spectrum of $CePd_{0.5}Rh_{0.5}Al$. The scalar relativistic spin-polarized calculations were carried out for two different geometries: in structure 1, space group *Pnma*, the atomic positions 4*c* are occupied by Ce1, Ce2; Rh, Pd; Al1, and Al2, respectively, while in structure 2 the atomic positions of Pd and Rh are switched. The atomic radii of Pd and Rh are similar, and hence in reality these atoms are statistically distributed over the same sites. As mentioned above, the main goal of these calculations was to identify the partial DOS contributions to the valence bands. However, even within this simple approach, it was possible to find out that the overall shapes of the XPS spectra are strongly sensitive to atom ordering. Further discussion of this issue requires more advanced theoretical modeling of the system (see, e.g., Ref. 57).

It is very likely that Pd and Rh atomic disorder at the 4*c* sites changes the J_{fc} coupling between Ce atoms, and just this effect could result in the spin-glass behavior in the $CePd_{1-x}Rh_xAl$ series. In classical spin glasses, random freezing of the magnetic moments arises due to the dominant RKKY exchange interaction between the randomly placed

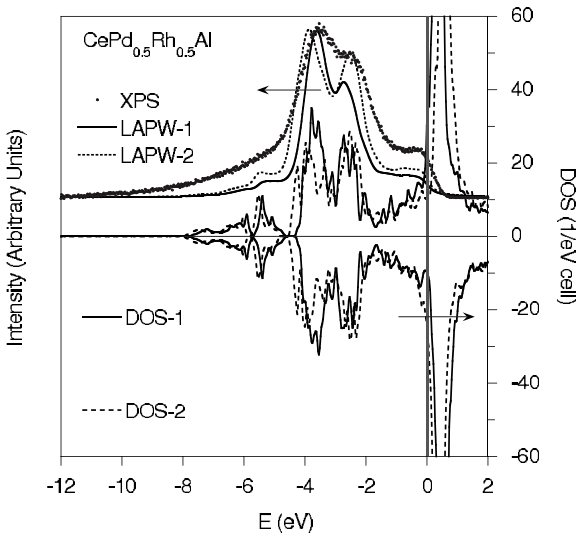

FIG. 9. Comparison of the DOS (LAPW) in $CePd_{0.5}Rh_{0.5}Al$ convoluted with Lorentzians of half-width 0.4 eV, taking into account proper cross sections for bands with different l symmetry, calculated for two different Pd-Rh configurations (structures 1 and 2) and the measured XPS VB spectra, with the background subtracted. Also shown is the spin-polarized total DOS in $CePd_{0.5}Rh_{0.5}Al$ derived from the LAPW calculations for the structures 1 and 2. The Fermi energy is at $E=0$.

magnetic moments. In the compounds studied, the Ce atoms occupy a periodic lattice, but the nonmagnetic elements (Pd, Rh, Al) if they are disordered, introduce a varying electronic environment around the Ce ions. As the Ce-Ce exchange interactions depend on the random occupation in the vicinity of the Ce ions, a spin-glass state would be possible at low temperatures, as evidenced in several other systems with structural disorder.[58] Recently, a statistical distribution of the Rh and Pd atoms over the same crystallographic sites was postulated to explain the weak magnetic anisotropy effect in the series $CePd_{1-x}Rh_x$.[19]

IV. SUMMARY

The present studies corroborated the antiferromagnetic order in CePdAl and indicated antiferromagnetism in the $CePd_{1-x}Rh_xAl$ alloys with $x>0.9$. For the Rh content $0<x\leq 0.9$ no long-range ordering was found. The results of the specific heat and electrical resistivity measurements hint at the formation at low temperatures of spin-glass-like states. Another possible explanation of the observed features might be itinerant-electron ferromagnetism, which is unlikely, however, because of the low-temperature magnetic properties of these alloys. The spin-glass behavior in the $CePd_{1-x}Rh_xAl$ series may be caused by random distribution of the Pd, Rh, and Al atoms in the crystallographic unit cell, which affects the exchange interactions between the Ce atoms (the nonmagnetic atom disorder mechanism). Similar effects of statistical distribution of the Rh and Pd atoms have recently been discussed for the $CePd_{1-x}Rh_x$ system.[19,20]

For some of the $CePd_{1-x}Rh_xAl$ alloys the Kondo effect was evidenced at low temperatures. It appears that its strength depends on the number of conduction electrons, which quasicontinuously decreases with rising Rh content. The Kondo screening is strong enough to be observed in the resistivity and specific heat data of samples with $x<0.6$. For alloys richer in Rh atoms ($0.6<x\leq 0.9$) this effect is partially quenched. The terminal compound CeRhAl is characterized as an antiferromagnetic Kondo lattice. In this material, however, an atomic disorder provokes unusual temperature dependences of the magnetic susceptibility and electrical resistivity above the temperature T_N. The magnetic ground state properties of CePdAl or CeRhAl can be explained in the framework of the Doradziński and Spałek theoretical approach. On the V-n_e plane of the DS diagram the compound CePdAl is located in the region of antiferromagnetic Kondo lattices, while CeRhAl lies on the line that separates the antiferromagnetic and ferromagnetic phases. Hence, in the entire system $CePd_{1-x}Rh_xAl$ antiferromagnetic ground states are more likely than ferromagnetic ones. However, the DS model is still rather simple and does not consider frustration effects or disordering, which both lead to the inhomogeneous magnetic states actually observed in the $CePd_{1-x}Rh_xAl$ series.

ACKNOWLEDGMENTS

The authors are grateful to Alicja Hackemer for her assistance in heat capacity measurements and Olgierd Żogał for his kind interest in this study. The authors are also very grateful to Józef Deniszczyk for discussion. The work was supported by the Ministry of Science and Higher Education through the Research Grants No. 1 P03B 052 28, No. 1 PO3B 094 30, and No. N202 038 31/1805. Parts of this work have been performed under the auspices of the COST P-16 European Network "Emergent Behaviour in Correlated Matter" and the National Scientific Network "Materials with Strongly Correlated Electrons."

[1] S. Doniach, Physica B & C **91**, 231 (1977); R. Jullien, J. N. Fields, and S. Doniach, Phys. Rev. B **16**, 4889 (1977); R. Jullien, J. Fields, and S. Doniach, Phys. Rev. Lett. **38**, 1500 (1977); C. Lacroix and M. Cyrot, Phys. Rev. B **20**, 1969 (1979).

[2] R. Doradziński and J. Spałek, Phys. Rev. B **56**, R14239 (1997); **58**, 3293 (1998).

[3] A. Ślebarski, J. Alloys Compd.. **423**, 15 (2006).

[4] A. Ślebarski, J. Goraus, A. Hackemer, and M. Sołyga, Phys. Rev. B **70**, 195123 (2004).

[5] T. J. Hammond, G. A. Gehring, M. B. Suvasini, and W. M. Temmerman, Phys. Rev. B **51**, 2994 (1995).

[6] N. H. Kumar and S. K. Malik, Phys. Rev. B **62**, 127 (2000).

[7] F. Hulliger, J. Alloys Compd. **196**, 225 (1993).

[8] C. Schank, F. Jährling, L. Luo, A. Grauel, C. Wassilew, R. Borth,

G. Olesch, C. D. Bredl, C. Geibel, and F. Steglich, J. Alloys Compd. **207-208**, 329 (1994).
[9] A. Dönni, G. Ehlers, H. Maletta, P. Fischer, H. Kitazawa, and M. Zolliker, J. Phys.: Condens. Matter **8**, 11213 (1996).
[10] K. Kamioka, A. Oyamada, K. Hashi, S. Maegawa, T. Goto, H. Kitazawa, and Y. Ysikawa, Physica B **259-261**, 121 (1999).
[11] S. Akamaru, Y. Isikawa, T. Kuwai, T. Mizushima, J. Sakurai, and Y. Uwatoko, Physica B **312-313**, 466 (2002).
[12] T. Goto, S. Hane, K. Umeo, T. Takabatake, and Y. Isikawa, J. Phys. Chem. Solids **63**, 1159 (2002).
[13] O. Gunnarsson and K. Schönhammer, Phys. Rev. B **28**, 4315 (1983); J. C. Fuggle, F. U. Hillebrecht, Z. Zolnierek, R. Lässer, Ch. Freiburg, O. Gunnarsson, and K. Schönhammer, *ibid.* **27**, 7330 (1983).
[14] W. Kraus and G. Nolze, J. Appl. Crystallogr. **29**, 301 (1996).
[15] P. Blaha, K. Schwarz, G. Madsen, D. Kvasnicka, and J. Luitz, computer code WIEN2K (Karlheinz Schwarz Techn, Universitat Wien, Austria, 2001).
[16] J. P. Perdew, K. Burke, and M. Ernzerhof, Phys. Rev. Lett. **77**, 3865 (1996).
[17] J. J. Yeh and I. Lindau, At. Data Nucl. Data Tables **32**, 1 (1985).
[18] D. X. Li, S. Nimori, H. Kitazawa, and Y. Shiokawa, Physica B **378-380**, 805 (2006).
[19] M. Deppe, P. Pedrazzini, N. Caroca-Canales, C. Geibel, and J. G. Sereni, Physica B **378-380**, 96 (2006).
[20] J. G. Sereni, R. Küchler, and C. Geibel, Physica B **359-361**, 41 (2005).
[21] U. Larsen, Phys. Rev. B **14**, 4356 (1976).
[22] K. H. Fischer, Z. Phys. B: Condens. Matter **42**, 27 (1981).
[23] P. J. Ford and J. A. Mydosh, Phys. Rev. B **14**, 2057 (1976).
[24] N. Rivier and A. E. Mensah, Physica B & C **91**, 8 (1977).
[25] K. H. Fischer, Z. Phys. B **34**, 45 (1979).
[26] A. J. Millis, Phys. Rev. B **48**, 7183 (1993).
[27] C. Pfleiderer, M. Uhlarz, S. M. Hayden, R. Vollmer, H. v. Löhneysen, N. R. Bernhoeft, and G. G. Lonzarich, Nature (London) **412**, 58 (2001).
[28] P. G. Niklowitz, F. Beckers, G. G. Lonzarich, G. Knebel, B. Salce, J. Thomasson, N. Bernhoeft, D. Braithwaite, and J. Flouquet, Phys. Rev. B **72**, 024424 (2005).
[29] N. V. Mott, J. Non-Cryst. Solids **1**, 1 (1968).
[30] F. G. Aliev, Physica B **171**, 199 (1991).
[31] R. Troć and A. M. Strydom, P. de V. du Plessis, V. H. Tran, A. Czopnik, and J. K. Cockroft, Philos. Mag. **83**, 1235 (2003).
[32] V. Ichas, J. C. Griveau, J. Rebizant, and J. C. Spirlet, Phys. Rev. B **63**, 045109 (2001).
[33] In the low-temperature spin-glass phase, the Kondo effect can be quenched (e.g., see Ref. 22) by high internal fields of frozen spins, whereas a high-temperature ln T term in the $\Delta\rho(T)$ data is expected to be reminiscent of the existence of the coherence in the Kondo lattice.
[34] Fu-sui Liu,W. A. Roshen, and J. Ruvalds, Phys. Rev. B **36**, 492 (1987).
[35] B. Cornut and B. Coqblin, Phys. Rev. B **5**, 4541 (1972).
[36] A. K. Bhattacharjee and B. Coqblin, Phys. Rev. B **13**, 3441 (1976).
[37] J. Tang, A. Matsushita, H. Kitazawa, and T. Matsumoto, Physica B **217**, 97 (1996).
[38] L. J. de Jongh and A. R. Miedema, Adv. Phys. **23**, 1 (1974).
[39] S. Süllow, G. J. Nieuwenhuys, A. A. Menovsky, J. A. Mydosh, S. A. M. Mentink, T. E. Mason, and W. J. L. Buyers, Phys. Rev. Lett. **78**, 354 (1997).
[40] D. X. Li, Y. Shiokawa, Y. Homma, A. Uesawa, A. Donni, T. Suzuki, Y. Haga, E. Yamamoto, T. Honma, and Y. Onuki, Phys. Rev. B **57**, 7434 (1998).
[41] A. Ślebarski, D. Kaczorowski, J. Głogowski, and J. Goraus (unpublished).
[42] J. M. D. Coey, S. von Molnar, and R. J. Gambino, Solid State Commun. **24**, 167 (1977); J. O. Thomson and R. J. Thompson, J. Phys. F: Met. Phys. **11**, 247 (1981); K. Binder and A. P. Young, Rev. Mod. Phys. **58**, 801 (1986).
[43] D. L. Martin, Phys. Rev. B **20**, 368 (1979).
[44] K. D. Schotte and U. Schotte, Phys. Lett. **55A**, 38 (1975).
[45] S. D. Bader, N. E. Phillips, M. B. Maple, and C. A. Luengo, Solid State Commun. **16**, 1263 (1975).
[46] C. D. Bredl, F. Steglich, and K. D. Schotte, Z. Phys. B **29**, 327 (1978).
[47] H.-U. Desgranges and K.D. Schotte, Phys. Lett. **91A**, 240 (1982).
[48] This assumption might be an oversimplification because of possible differences in the phonon spectra of the Ce- and La-based counterparts, resulting from different atomic masses and frequencies $\omega \sim (C/M)^{1/2}$. However, at low temperatures, say below 7 K, the lattice contribution to the specific heat is anyway almost negligible.
[49] A. Hewson, *The Kondo Problem to Heavy Fermions* (Cambridge University Press, Cambridge, U.K., 1993).
[50] P. W. Anderson, Phys. Rev. **124**, 41 (1961).
[51] S. Tougaard and P. Sigmund, Phys. Rev. B **25**, 4452 (1982).
[52] S. Doniach and M. Šunjić, J. Phys. C **3**, 285 (1970).
[53] A. Ślebarski, T. Zawada, J. Spałek, and A. Jezierski, Phys. Rev. B **70**, 235112 (2004).
[54] M. Gamża, A. Ślebarski, and H. Rosner, J. Phys.: Condens. Matter **20**, 025201 (2008).
[55] The Ce 3*d* XPS spectra allow estimation of the occupation number n_f, and the energy Δ within an accuracy of the order of 15%. The errors are due to the uncertainties in the intensity ratios $3d^9f^0:3d^9f^1:3d^9f^2$, which can be attributed to the uncertainty in the spectral decomposition, the background subtraction, and the approximations in the Gunnarsonn-Schönhammer theory.
[56] A. J. Signorelli and R. G. Hayes, Phys. Rev. B **8**, 81 (1973).
[57] A. Zunger, S.-H. Wei, L. G. Ferreira, and J. E. Bernard, Phys. Rev. Lett. **65**, 353 (1990).
[58] K. A. Gschneidner, Jr., J. Tang, S. K. Dhar, and A. Goldman, Physica B **163**, 507 (1990).